PCCP

Accepted Manuscript

Vibronic coupling in the excited-states of carotenoids

Takeshi Miki,[1] Tiago Buckup,[1] Marie S. Krause,[1] June Southall[2], Richard J. Cogdell[2] and Marcus Motzkus[1]

[1]*Physikalisch-Chemisches Institut, Ruprecht-Karls-Universität Heidelberg, D-69120*

Heidelberg, Germany

[2]*College of Medical, Veterinary, and Life Science, University of Glasgow, G12 8QQ*

Glasgow,

Scotland, United Kingdom

*E-mail   marcus.motzkus@pci.uni-heidelberg.de;   tel.   (+49)6221548727;   fax (+49)6221548730.

1

ABSTRACT

The ultrafast femtochemistry of carotenoids is governed by the interaction between electronic excited states, which has been explained by the relaxation dynamics within a few hundred femtoseconds from the lowest optically allowed excited state S_2 to the optically dark state S_1. Extending this picture, some additional dark states ($3A_g^-$ and $1B_u^-$) and their interaction with S_2 state have been also suggested to play a major role in the ultrafast deactivation of carotenoids and their properties. Here, we investigate the interaction between such dark and bright electronic excited states of open chain carotenoids, particularly its dependence on the number of conjugated double bonds (N). We focus on the ultrafast wave packet motion on the excited potential surface, which is modified by the interaction between bright and dark electronic states. Such a coupling between electronic states leads to shifts of the vibrational frequency during the excite-state evolution. In this regard, pump-degenerate four-wave mixing (pump-DFWM) is applied to a series of carotenoids with different number of conjugated double bonds $N = 9$, 10, 11 and 13 (neurosporene, spheroidene, lycopene and spirilloxanthin, respectively). Moreover, we demonstrate in closed-chain carotenoid (lutein) that the coupling strength and therefore the vibrational shift can be tailored by changing the energy degeneracy between the $1B_u^+$ and $1B_u^-$ states via solvent interaction.

1. INTRODUCTION

The interaction between molecular electronic states plays a central role in understanding the photophysical and photochemical molecular properties. Couplings between energetically close-lying electronic states may lead to, for example, the formation of conical intersections and to ultrafast deactivation processes in the excited states of molecules.[1] Moreover, couplings between states with different transition dipole moments may enhance the transition dipole moment of weaker transitions by intensity borrowing.[2] Coupling between electronic states are not restricted, however, to energetic degenerate states. Electronic states may still show vibronic coupling effects even when the states are energetically well separated by more than thousands of wavenumbers.[3] In general, coupling phenomena are particularly important the larger the molecule becomes, due to the increased number of degrees of freedom and close-lying electronic states.

Biopolyenes, like carotenoids, are examples of such large polyatomic systems. Several types of couplings between electronic states have been described for carotenoids. The electronic states of all-*trans* carotenoids have been usually described by geometrical features of the π-electron conjugated systems with C_{2h} symmetry.[4-6] In this representation, the two low-lying electronic states (S_0 and S_1) have the same geometry, A_g, and show a strong adiabatic vibronic coupling due to the A_g C=C stretching mode.[3] The coupling between the $1A_g^-$ (S_0) and $2A_g^-$ (S_1) states in carotenoids leads to the well-known frequency increase of about $100 - 150$ cm^{-1} for the C=C in S_1. While the effect of such adiabatic vibronic coupling between the ground and the first excited state is well understood[7] and has been experimentally observed by several experimental techniques,[8-10] the coupling between the excited electronic states of carotenoids is still not clear.

The S_2 electronic state has $1B_u^+$ symmetry and is the first one-photon allowed electronic state from the ground state. The experimentally observed ultrafast deactivation between the $1B_u^+$

(S$_2$) and 2A$_g^-$ (S$_1$) takes place within about 200 fs and has been claimed as an evidence for a very efficient relaxation channel between the two potential surfaces[11-16]. Although this simple deactivation picture (S$_2 \rightarrow$ S$_1$) can explain the ultrafast experimental deactivation constants and the almost lack of dependence of this deactivation constant on the carotenoid's number of conjugated double bonds (*N*), it fails to explain several observations of resonant-Raman experiments,[17] fluorescence[18] and quantum beatings in pump-probe experiments.[19] In this regard, it has been long debated whether the S$_2$ state relaxes directly to the S$_1$ state or via other electronic excited states are present between these two states.[20, 21] Electronic states with 1B$_u^-$ and 3A$_g^-$ symmetry have been suggested to be energetically close to the S$_2$ state depending on number of conjugated double bonds (Fig. 1)[5, 6, 22-25] and to strongly couple to the S$_2$ state in some cases.[19, 26-29] The electronic coupling between the 1B$_u^+$ and 1B$_u^-$ has been further suggested to be responsible for strong coherent oscillatory contributions to the population signal in transient absorption when the 1B$_u^+$ (S$_2$) state was excited from the 1A$_g^-$ (S$_0$) state for lutein (*N* ~ 10) and all-*trans*-*β*-carotene (*N* ~ 10).[19] Since the energetic position of the 1B$_u^+$ state depends on the solvent polarizability,[20, 21, 30] which therefore modifies the crossing of the 1B$_u^+$ and 1B$_u^-$ potential surfaces and the strength of the coupling between them, the oscillatory contribution[19] and the associated dynamics have been shown to be dependent on the solvent.[28] All these effects have been only reported for lutein, spheroidene and all-*trans*-β-carotene, carotenoids with about 10 conjugated double bonds. For carotenoids with *N* ~ 10, modern calculations based on the combination of multireference configuration interactions with density functional theory states that the 3A$_g^-$ is energetically higher than the 1B$_u^+$ (S$_2$) (more than 1 eV for all-*trans*-*β*-carotene) and, therefore, does not play any role in the relaxation dynamics.[31, 32] These results contrast to the experimental results obtained for open-chain carotenoids with a similar number of conjugated double bonds *N* (Fig. 1),[22] suggesting that the energy of electronic excited states in open- and closed-chain carotenoids may show a different dependence on the number of conjugated double bonds *N*.

4

In spite of the fact that some sort of coupling seems to be present between the electronic states of carotenoids with conjugated double bonds around $N \sim 10$, it is still not clear whether such coupling should be described in the framework of an adiabatic vibronic coupling or diabatic mixing. The answer to that question may reside perhaps on analyzing how vibrational frequencies changes with the number of conjugated double bonds. Both kinds of coupling predict an energy up- as well as down-shift of the involved vibrational states, but they differ, however, on the symmetry selection rules for the coupled states: While adiabatic vibronic coupling follows the pseudoparity selection rule, i.e. states of "minus" type can couple to "minus" states, but not to "plus" states,[3] diabatic mixing just takes place between B_u states, and not between B_u and A_g states[27]. In this situation, since the separation between B_u and A_g states changes systematically for different conjugation lengths (Fig. 1), a measurement of how the vibrational frequency changes with the conjugation length should distinguish which coupling mechanism is present.

In this work, we focus on following the vibrational dynamics directly after S_0-S_2 excitation with high time resolution. We apply pump-degenerate four wave mixing (pump-DFWM)[10, 33-37] to a series of carotenoids with varying conjugated double bonds between $N = 9$ and 13. Depending on the number of conjugated double bonds, we will show that the shift of the C=C and C-C frequencies in the first 200 fs can be explained by the strong diabatic mixing between the $1B_u^-$ and $1B_u^+$ states. Moreover, by carefully changing the solvent, the strength of this coupling can be fine-tuned and, therefore, the vibrational dynamics can be modified.
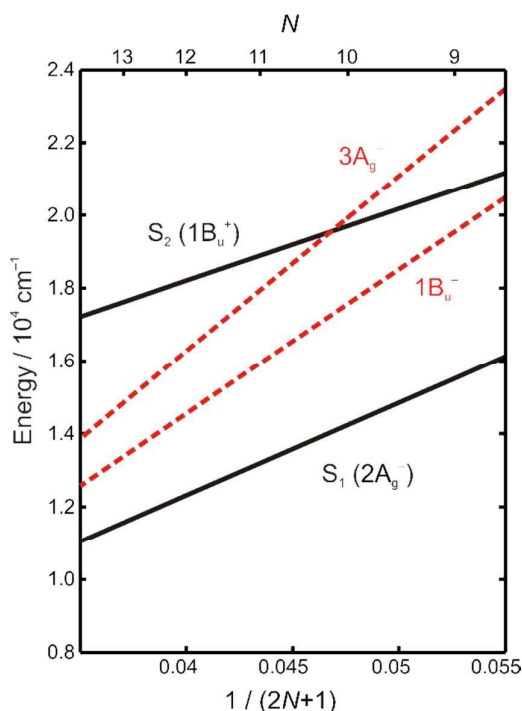
Figure 1 – Electronic states of carotenoids and their dependence on the number of conjugated double bonds (N). Data obtained from reference. [22]

2. EXPERIMENTAL METHODS

2.1 Sample preparation

The all-*trans*-carotenoids, namely neurosporene, spheroidene and spirilloxanthin, were extracted from *Rhodobacter sphaeroides* G1C, *Rhodobacter sphaeroides* 2.4.1 and *Rhodosprillum rubrum* S1, respectively. Lycopene and lutein were extracted from tomato and spinach by the following procedure. 100 g of powdered tomato or spinach were dissolved into 200 mL of acetone and percolated to obtain the solvent part. The process was repeated three times and all of the pigment mixture were evaporated to replace the solvent with acetone/hexane (1/1, v/v). The first column chromatography with Silica gel (Merck, Silica gel 60) was done to remove chlorophylls roughly. The pigment mixture was dried up with rotary evaporator and separated by a pair of alumina column chromatography (Merck, Aluminium oxide 90 standardized) and Silica gel column chromatography. 30 – 60 % acetone in hexane

6

was used as stepwise gradient developer. The purification process was performed twice. Pure carotenoids were dissolved into hexane with small amount of THF and recrystallized under -25^0C. The crystals were washed by hexane before dissolving the solvent for the measurement.

Carotenoids (neurosporene, spheroidene, lycopene and spirilloxanthin) were diluted into THF to be an OD = 2.0 in 1.0 mm path at the 0-0 transition peak. Lutein samples were dissolved into three different solvents: with hexane (Lu/Hex), THF (Lu/THF) or benzene (Lu/Bz) to obtain OD = 1.6 in a 1.0 mm path at the 0–0 transition peak. All solutions were filtered through a syringe filter (KY61.1, Rotilabo). During the measurement, the sample was exchanged continuously via flow cell. The stability of the sample was checked by measuring the stationary absorption spectra before and after measurement.

2.2 Experimental setup

Transient absorption (TA) and pump-DFWM measurements were performed with the experimental setup already reported.[35] Briefly, it consists of a Ti: Sapphire laser which generates 120 fs, 690 μJ pulses with 1 kHz repetition rate centered at 795 nm. The output was split equally into two parts to pump two non-collinear optical parametric amplifiers (nc-OPA). An initial pump pulse (k_{IP}) was generated in the first nc-OPA with a spectrum near-resonant with the S_0-S_2 transition (Fig. 2). Pulse duration was about 17 fs with typical energies of about 60 nJ. The output of the second nc-OPA was tuned resonant with the S_1-S_N excited state absorption (Fig. 2) and pulse duration was about 13 fs. This output was split into three beams, named pump (k_{pu}), Stokes (k_{St}) and probe (k_{pr}). These beams were focused on the sample with a folded BOXCARS geometry[38]. Energies of about 20-25 nJ were used for each beam.
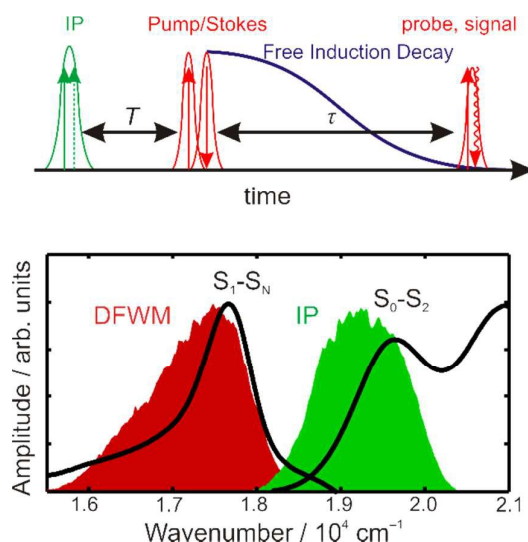
Figure 2 - Pulse sequence and spectra for Pump-DFWM. Initial pump (green) and DFWM (red) spectra were adjusted to be overlapped with S_0-S_2 and S_1-S_N transition, respectively.

Time-resolved signals were recorded as a function of the initial pump delay (T) and of the probe delay (τ) (Fig. 2). Delay between pump and Stokes pulses was set to zero. Measurements were performed with 40 laser shots per data point with 3 times averaging. The pump-DFWM signal was detected by using photomultipliers with 10 nm bandwidth interferometric filters at selected wavelengths.

2.3 Data analysis

Pump-DFWM spectroscopy is a multi-dimensional technique that allows us to observe electronic and vibrational evolution in two time axes T vs. τ.[37] Each transient at each T step contains oscillatory and non-oscillatory contributions. Those contributions were separated by polynomial fitting in the region after probe delay $\tau > 100$ fs. Vibrational spectra were obtained by fast Fourier transformation (FFT) of oscillatory contribution after zero-padding, windowing and apodization. Central vibrational frequencies were evaluated by Gaussian fitting. Experimental uncertainty in the determination of central frequencies is about 5 cm^{-1}, which is mainly due to the fitting of the broad Fourier spectral features and not due to the

precision of the piezos used to scan the delay. The transient absorption data was analyzed by singular value decomposition (SVD) after dispersion correction. The linear mapping with coefficient matrix (C-matrix) was performed until more than 95 % of the reconstituted spectra are obtained.[39, 40]

3. RESULTS AND DISCUSSION

3.1 Pump-DFWM 2D Transient Signals

Pump-DFWM data was acquired for four carotenoids with different numbers of conjugated double bonds ($N = 9$, 10, 11 and 13) (Fig. 3). The DFWM spectrum was carefully selected to spectrally overlap with the excited-state absorption red-shifted from the S_0-S_2 transition (see Fig. 2), i.e. it was electronically *non*-resonant with the S_0-S_2 transition for each carotenoid. Therefore, ground-state contributions under these conditions were orders of magnitude smaller than the electronically resonant DFWM signal generated from the electronically excited states.
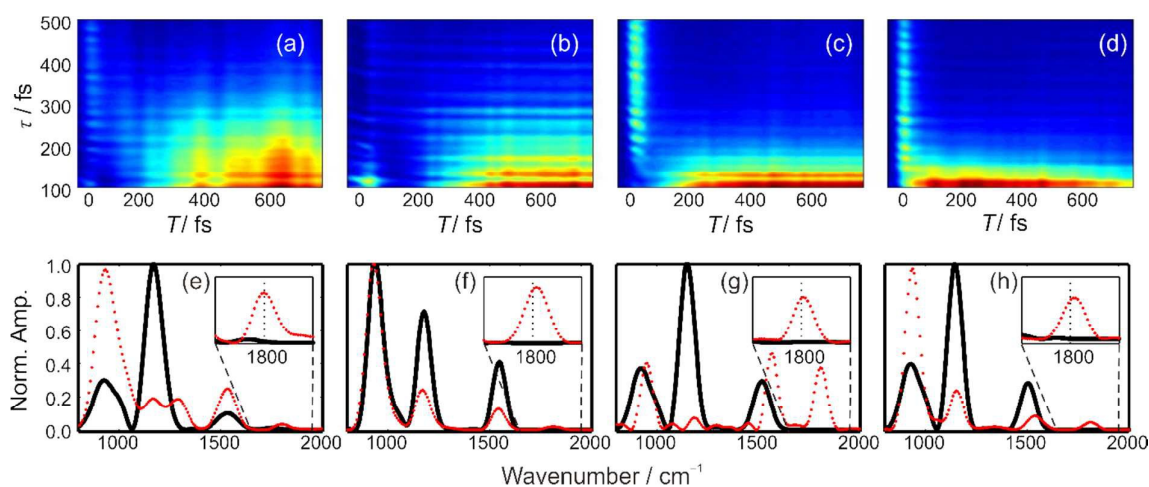
Figure 3 – (a)-(d) Pump-DFWM signal collected for carotenoids with $N = 9$, 10, 11 and 13, respectively. Data was detected at $\lambda_{det} = 570$, 600, 630 and 660 nm for $N = 9$, 10, 11 and 13, respectively. The intensity of the signal increases from cold color (blue) to hot color (red). (e)-(h) The vibrational spectra were calculated from

oscillatory transients measured at $T = 25$ fs (black) and 700 fs (red). The four spectra at $T = 700$ fs were multiplied by about a factor 70 for comparison.

The Pump-DFWM signal contains a *non-oscillatory* and an *oscillatory* contribution. The basic features of this technique on biopolymers have been described in detail in references [35-37]. Figure 4 shows schematically a typical T-τ scan, which exhibits for clarity the three characteristic contributions observed experimentally (Fig. 3). In general, the *non-oscillatory* contribution shows similar transient features for all carotenoids investigated here (Fig. 3 top). At very early *T*-delays (< 30 fs) between the initial pump and the DFWM sequence, a long living signal along the τ-delay appears. At later *T*-delays, the signal decays much faster, typically with time constants shorter than 300 fs. The long dynamics at early *T*-delays have been explained in previous works by a stimulated emission pumping mechanism (region I in Fig. 4),[10, 41] well-known to be resonant with S_2-hot-S_0 transitions of not only carotenoids, but also retinoids as well as other molecular systems with strong fluorescence emission transitions.[42-45] The very fast decay of the signal along τ-delay at later *T*-delays contains several contributions from the excited states e.g. the S_1-S_n transition (region II in Fig. 4). Spheroidene ($N = 10$), and in some extent also neurosporene ($N = 9$), shows an additional signal contribution at very early *T*-delay, which is, however, extremely short lived along the τ-delay (region III in Fig. 4). This signal stems from a contribution from an electronic dark state directly after the S_2 state relaxation.[36]
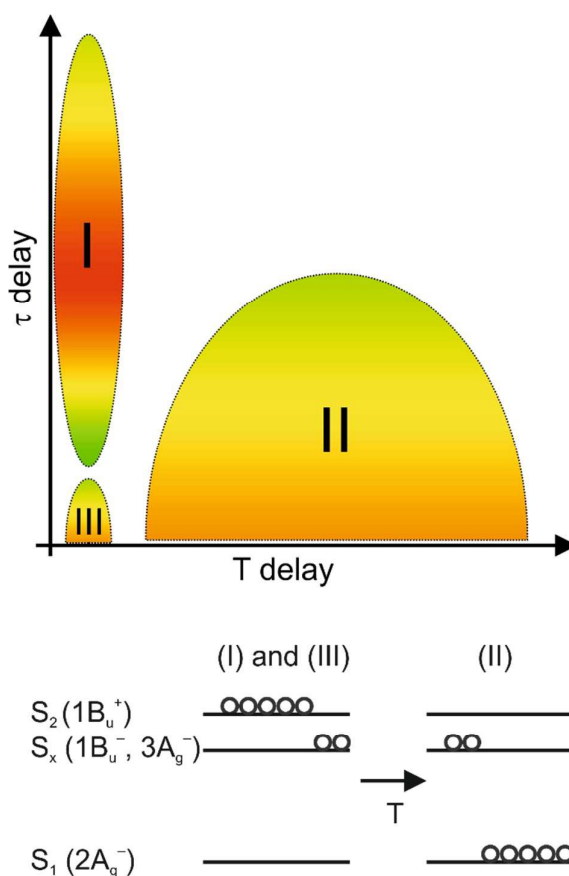
Figure 4 –TOP: Schematic temporal evolution and relevant electronic states of the main contributions to the Pump-DFWM signal of carotenoids.[10, 36, 37] I – Stimulated emission pumping between the excited electronic state and the hot-ground state. II – Contributions from the S_1-S_n transitions. III – Short-lived pump-DFWM generated close to the Franck Condon region. Region III appears only for carotenoids with conjugation length around 10 and is specific for a transition of a dark state.[36] BOTTOM: Corresponding temporal evolution of the population in the electronic excited states. Initially, population is mainly in the states S_2 and S_x (contributions I and III), while at later T-delays, population relaxes towards the S_1-state (contributions II).

The *oscillatory* contributions contain a well-defined group of high-frequency modes present for all carotenoids (Fig. 3 bottom). Four main sets of frequencies can be detected: Frequencies between $1150 - 1200 \text{ cm}^{-1}$ and $1500 - 1600 \text{ cm}^{-1}$ are assigned to the fundamental C-C and C=C stretching mode, respectively.[46, 47] Frequencies at about 915 cm^{-1} come from the solvent (THF, in this case) and their detection in Raman based experiments has been explained to be

due to beating between chromophore and solvent optical polarizations[48] and due to intermolecular vibronic coupling between solvent and carotenoid molecular hyper-polarizabilities.[49] An additional frequency at about 1800 cm^{-1} can be also detected for all carotenoids, which is a well-known consequence of the coupling between the S_0 and S_1 states due to their Ag symmetry.[7, 30] This coupling increases the vibrational frequency of central C=C stretching in the S_1 state, while the frequency of the peripheral C=C stretching in the S_1 state is not shifted, and has been observed before by other experiments.[46, 47]

3.2 Evolution of Molecular Vibrational Frequencies

The frequency of the C-C and C=C stretching modes during the deactivation of the excited electronic states is, however, not static. There are two main vibrational evolutions to consider. The first one is the change of the C-C and C=C stretching mode *frequencies* with the *T*-delay (Fig. 5). Carotenoids with a smaller number of conjugated double bonds ($N = 9$ and 10) show a down-shift of the frequency in the initial 100 fs, while carotenoids with $N = 11$ and 13 show an up-shift of the frequencies. For example, neurosporene ($N = 9$) shows a down-shift of the C=C stretching mode from about 1580 to about 1510 cm^{-1}. Contrasting to that, spirilloxanthin ($N = 13$) shows an up-shift from about 1510 to about 1530 cm^{-1}.
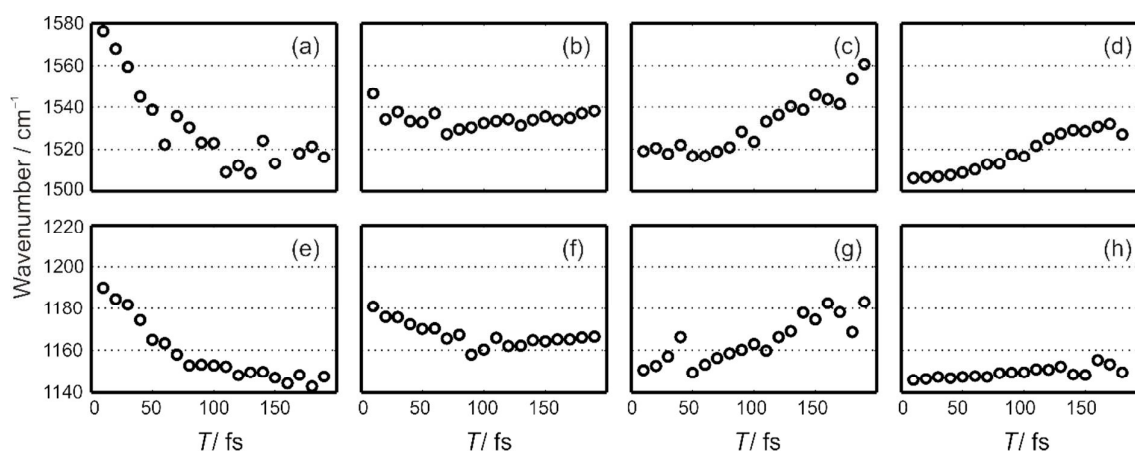
Figure 5 – Initial dynamics of the frequency of the (a)-(d) C=C and (e)-(h) C-C stretching modes for carotenoids with $N = 9$ (1st column), 10 (2nd column), 11 (3rd column) and 13 (4th column). Spectra were obtained Fourier transformation of transients between $\tau = 100$ and 550 fs.

The second important aspect in the vibrational dynamics in the excited state is the evolution of the C=C stretching mode at 1800 cm^{-1} (Fig. 6). Contrary to other C-C and C=C modes at 1160 cm^{-1} and 1500 cm^{-1}, this high-frequency mode is not present in the dynamics at early T-delays. The amplitude of the vibrational frequency rises with the T-delay and reaches its maximum after several hundreds of femtoseconds. In general, the shorter the carotenoid, the slower is its rise dynamics: The amplitude of this mode in spirilloxanthin ($N = 13$) increases with a time constant faster than 200 fs, while for spheroidene ($N = 10$), the rise time is much slower (> 500 fs). The central frequency of this mode also changes in time, but all carotenoids showed a comparable upshift of the frequency during the evolution over the initial 800 fs (Fig. 6). The dynamics of this mode in neurosporene ($N = 9$) was not possible to resolve due to its low amplitude, and, therefore, a fitting was not conclusive.
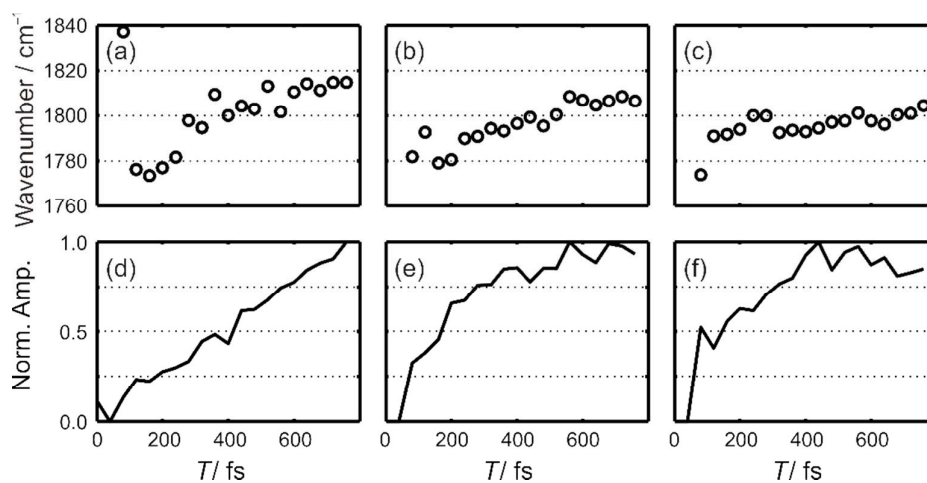
Figure 6 – Initial dynamics of (a)-(c) frequency and of the (d)-(f) amplitude of the C=C specific to S_1 state for carotenoids with $N = 10$ (1st column), 11 (2nd column) and 13 (3rd column). Spectra were obtained by Fourier transformation of transients between $\tau = 100$ and 550 fs.

It is important to compare the frequencies of these vibrational modes at selected T-delays with pure ground-state frequencies obtained with other techniques (see Table 1). Pure ground-state

C-C and C=C stretching modes obtained with resonant Raman measurements have lower wavenumbers when compared to similar vibrational modes detected at later T-delays, i.e. when the S_1 state is populated ($T = 700$ fs). Furthermore, a comparison of the wavenumber values for late T-delays among the carotenoids shows that the wavenumber of the C=C stretching mode increases in the S_1-state, the longer the carotenoid is: This wavenumber varies from 1532 cm^{-1} ($N = 9$) up to 1564 cm^{-1} ($N = 11$). An exception for this observation is spirilloxanthin ($N = 13$), which shows a wavenumber (1534 cm^{-1}) similar to neurosporene (1537 cm^{-1}). A similar trend can be observed for the C-C stretching mode increases in the S_1-state.

Table 1 – Vibrational wavenumbers of C-C and C=C modes for several open- and closed –chain carotenoids with N = 9, 10, 11 and 13. All wavenumber units are in cm^{-1}.

Open Chain	This work									Literature		
	T=700fs			T=25fs – τ=100-470fs			T=25fs – τ=200-570fs					
	C-C	C=C	C=C S$_1$	C-C	C=C	C=C S$_1$	C-C	C=C	C=C S$_1$	C-C	C=C	C=C S$_1$
Neurosporene (N=9)	1163	1537	1803	1181	1551	-	1156	1539	-	1151 (S$_0$)[A]	1515 (S$_0$)[A]	1780 (S$_1$)[A]
Spheroidene (N=10)	1173	1545	1813	1178	1542	-	1166	1534	-	1150 (S$_0$)[B]	1516 (S$_0$)[B]	1794 (S$_1$)[B]
Lycopene (N=11)	1180	1564	1803	1158	1516	-	1150	1519	-	1143 (S$_0$)[B] 1140 (S$_1$)[E]	1501 (S$_0$)[B] 1513 (hot-S$_0$)[E] 1530 (S$_1$)[E]	1783 (S$_1$)[B]
Spirilloxanthin (N=13)	1150	1534	1802	1147	1506	-	1147	1508	-	1148 (S$_0$)[C]	1505 (S$_0$)[C]	1770 (S$_1$)[C]
Closed Chain												
β-Carotene (N~10.5)	1140[F]	1528[F]	1765[F]	1160[F]	1535[F]	-	-	-	-	1160 (S$_0$)[D] 1145(hot-S$_0$)[D] 1190 (S$_1$)[D]	1526 (S$_0$)[D] 1515 (hot-S$_0$)[D] 1540 (S$_1$)[D]	1785 (S$_1$)[D]
Lutein (N~10.5)	1135	1535	1783	1153	1524	-	1153	1522	-			

[A] Resonant Raman in benzol.[50]
[B] Resonant Raman in benzol.[17]
[C] Resonant Raman in n-hexane.[51]
[D] Pump-DFWM and -IVS in THF.[35]
[E] Pump-DFWM in THF.[34]
[F] Pump-DFWM in THF.[33]

3.3 Effect of Overlapping Contributions on the Evolution of Frequencies

In order to understand the evolution of the frequencies after the S$_0$-S$_2$ excitation with initial pump, it is important to discuss the role of temporally overlapping contributions on the experimentally detected frequencies. The spectrum of DFWM pulses defines which optical transitions are probed after the initial excitation by the initial pump pulse.[37] At T-delays shorter than 30 fs, transitions between the excited electronic states near the Frank-Condon region and hot-S$_0$ play a major role in the signal generation (contribution I in Fig.4). Thus molecular vibrational modes from hot-S$_0$ as well as from electronically excited states (S$_2$ or any other dark state near to S$_2$) may contribute to the signal. For early delay times beyond this initial time window (T > 30 fs), processes involving the S$_2$-hot-S$_0$ transition are suppressed, and transitions resonant with excited state absorptions of dark states like the 3A$_g^-$ and 1B$_u^-$ contribute to the signal (contribution III in Fig.4). At much later T-delays, the S$_1$-state will eventually be populated and optical transitions involving the S$_1$-state will be the major signal

15

source (contribution II in Fig.4). The dynamics of these contributions is of course a continuous process, where each detection window along the T-delay overlaps partially with the neighbouring ones. This makes the analysis very challenging in one-dimensional techniques like transient absorption, because it does not allow an unambiguous isolation of the vibrational frequency of a given electronic state during the activation. Multidimensional time-resolved spectroscopies like pump-DFWM or pump-IVS, however, provide multiple time axes, where the dynamics can be followed and potentially overlapping molecular dynamics can be disentangled. This can be done by applying a sliding window Fourier transformation at specific time windows (Fig. 7).

This principle can be applied to the overlapping molecular vibrational modes at $T < 30$ fs from hot-S_0 and electronic excited states by using the additional probe-axis τ of DFWM: While vibrational modes in the long-living hot-S_0 state dephases with the time scale of ground-state process (over a few picoseconds), vibrational coherence that originate from short-living electronically excited states must dephase as fast as the population decays. Therefore, at about $T = 25$ fs, by performing sliding window Fourier transformations of early τ-delays (e.g. 100-470fs), vibrational coherences from hot-S_0 as well as from short-living electronic states will contribute, while sliding window Fourier transformations of late τ-delays contain exclusively hot-S_0 vibrational modes (200-570fs), since vibrational coherence from the electronic excited states has already dephased (Fig.7). Note that the values obtained at early τ-delays will be interpreted as an average of the vibrational frequencies of the S_2 state and of the hot-S_0.
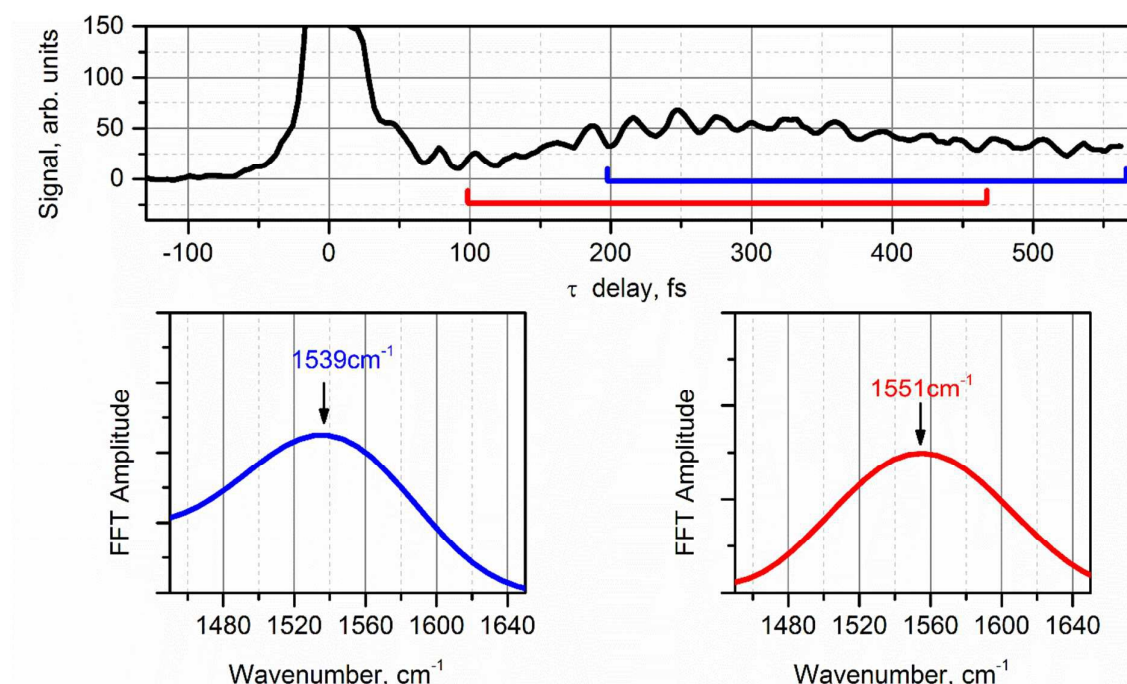
Figure 7 – Disentangling overlapping contributions in multidimensional time-resolved vibrational spectroscopy by using sliding window Fourier transformation at specific T-delay. The blue FFT spectrum was obtained by transformation of the transient between $\tau = 200$fs and 570fs, while the red FFT spectrum was obtained by transformation of the transient between $\tau = 100$fs and 470fs.

3.4 Couplings between Electronic States

The results presented in section 3.2 clearly show that (i) the frequency changes of the C-C and C=C stretching modes depend on the carotenoid conjugation length and (ii) the C=C S_1 (1800cm^{-1}) stretching mode does not follow that dependence. Before we focus on these two experimental findings in more detail, it is important to discuss the probing step in the pump-DFWM process. The DFWM sequence probes the transient population (and potentially also vibrational coherence) induced by the initial pump. It does that by generating a vibrational wave packet at a given point of a potential surface during the population deactivation. A wave packet generated this way involving initially high-lying vibrational levels of, for example, an anharmonic potential will have initially a lower frequency than a wave packet generated involving low-lying vibrational levels of the same potential (see also the scheme for the

potential anharmonicity after relaxation at later T-delays at Fig. 11). If the frequencies of these two wave packets are compared, the respective vibrational frequency will show an up-shift of the frequency as the system relaxes within this anharmonic potential. The higher the anharmonicity of the electronic potential associated, the higher the measured up-shift would be. This is exactly the case for the up-shift of the frequency of the C=C S_1 stretching mode at about 1800 cm^{-1}, which is restricted to the S_1 state in carotenoids and can be explained in the framework of a wave packet generated on an anharmonic potential (Fig. 6 and Fig.11). The rise time constant of this mode is slower in spheroidene ($N = 10$) than in spirilloxanthin ($N = 13$) in agreement with the slower population built up of the S_1-state.[30] Moreover, the magnitude of the frequency up-shift of about 30 – 40 cm^{-1} suggests an S_1 potential with weak anharmonicity. By assuming that the S_1 state is populated mainly via the fourth vibrational level (v = 3),[8, 52] the anharmonic constant for the S_1-state can be estimated to be about 0.002 – 0.005.

The origin of the C=C S_1 stretching mode at about 1800 cm^{-1} has been explained as a consequence of anharmonic vibronic coupling between the $1A_g^-$ and the $2A_g^-$ states induced by the total symmetric C=C stretching mode.[3, 7] This coupling has not only the effect of inducing a new C=C frequency in the $2A_g^-$ state (the 1800 cm^{-1}), but also leads to a decrease of the C=C frequency in the $1A_g^-$ state.[3] As can be seen in table 1, the longer the carotenoid's conjugation length, the lower is the frequency of the C=C mode in the ground state. This can be understood, since the anharmonic vibronic coupling between A_g states gets stronger for energetically closer lying electronic states. For carotenoids with shorter conjugation lengths such as neurosporene, the energy separation between the Ag states is higher than for carotenoids with longer conjugation lengths, therefore, the coupling is weak and the frequency of the C=C stretching mode in the $1A_g^-$ state (1539 cm^{-1}) is the same as in the $2A_g^-$ state (1537 cm^{-1}) within the experimental precision. This contrasts to spirilloxanthin, what shows a frequency of 1534 cm^{-1} for the $2A_g^-$ state and 1508 cm^{-1} for the ground state.

The anharmonic vibronic coupling behind the generation of the new C=C frequency at about 1800 cm^{-1} takes place only between electronic states of A_g symmetry.[3, 7] Thus, the frequency of the C=C mode of the energetically closer $1B_u^+$ state is not affected by this type of coupling, which matches the experimental observation that the amplitude of the new C=C mode rises with the population of the $2A_g^-$ state (Fig. 6). An important exception to that has been reported for spheroidene, which displayed an additional frequency around 1800 cm^{-1} with small amplitude at very early *T*-delays (not explicitly shown here).[36] This has been explained due to the coupling of $2A_g^-$ and $3A_g^-$ states, which seems to take part in the $1B_u^+$ relaxation for $N = 10$. The presence of this mode for an open-chain carotenoid with $N = 10$ contrasts with the numerical calculations performed for closed chain carotenoids also with $N = 10$, like lutein and β-carotene. For these carotenoids, the $3A_g^-$ is well above the $1B_u^+$ state, which rules out any possibility of detection of this state in the dynamics after the $1B_u^+$ excitation. The fact that the $3A_g^-$ vibrational dynamics can be detected for spheroidene, just underlines that open- and closed-chain carotenoids may not be so straightforwardly compared regarding their vibrational and electronic dynamics.

The down-shift of a vibrational frequency during the relaxation within a single electronic potential cannot be explained, however, by anharmonicity effects as above. Vibrational frequency down-shifts must necessarily involve vibrational states with decreasing separation during the dynamics (see also the scheme of diabatic mixing for earlier T-delays at Fig. 11). The initial frequency down-shifts of the C=C and C-C modes for neurosporene and spheroidene, and the absence of that for the longer carotenoids (lycopene and spirilloxanthin) (Fig. 5), gives a hint of the origin of the experimental down-shift (Fig. 11). The two carotenoids with shorter conjugation length can be mainly distinguished from the two carotenoids with longer conjugation length by the energy separation between the $1B_u^+$ and the $1B_u^-$ states: the energy gap between these two states is smaller in the former case. The proximity and interaction of these two B_u states has been evoked as the origin of resonant

Raman[17] and fluorescence[18] profiles for several carotenoids with similar conjugation lengths. The degeneracy between vibrational levels of these two states leads to a strong diabatic mixing and a splitting of the degenerate vibrational levels: The closer they are energetically, the bigger is the splitting. It is very important to note that such diabatic mixing only takes place between states with B_u-symmetry.[27]

The energy separation between $1B_u^+$ and $1B_u^-$ states increases with the carotenoid length, therefore, one would expect that the diabatic mixing gets weaker the longer the conjugation length gets. In this situation, one also expects that as the diabatic mixing becomes weaker, the up-shift of vibrational frequency should become increasingly observable due to the evolution on the anharmonic excited potentials. The experimental data demonstrates exactly this scenario: In neurosporene, the $1B_u^+$ and $1B_u^-$ states are strongly degenerate and the down-shift due to the diabatic mixing is strong. As the separation between these B_u states increase for increasing N, this diabatic mixing gets weaker and an up-shift due the anharmonic potential takes over. This can be clearly observed for lycopene and spirilloxanthin which show no frequency down-shift at all of the C-C and C=C stretching modes.

The interplay between the diabatic mixing and the evolution of the wave packet on the anharmonic potential can also be followed in the time domain by measuring the long-time dynamics of the frequency shift for T-delays up to 800 fs (compare to Fig.5, for example). This reveals that as the system relaxes away from the FC-region at $T = 0$ fs, the effect of the diabatic mixing between the B_u states gets weaker, and an frequency up-shift dynamics starts appearing as the system relaxes to the bottom of the S_1 state potential. This can be observed for neurosporene for both C-C and C=C stretching modes, while for lycopene, where diabatic mixing seems to play a minor role, only a frequency up-shift due to the evolution on an anharmonic potential can be observed (Fig. 8).
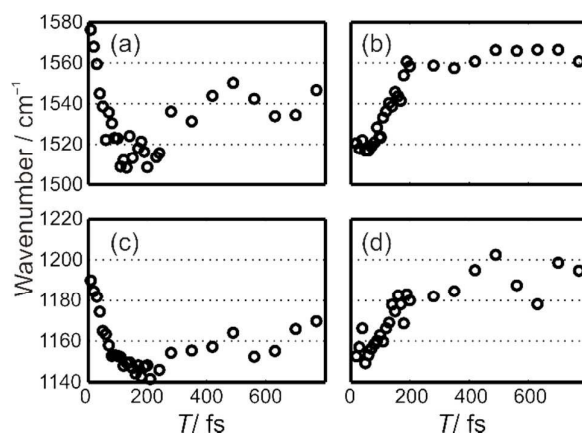
Figure 8 – Evolution of the vibrational frequency of the (a)-(b) C=C and (c)-(d) C-C stretching modes for neurosporene ($N = 9$) (1st column) and lycopene ($N = 11$) (2nd column) between $T = 0$ and 800 fs. Spectra was obtained by Fourier transformation of transients between $\tau = 100$ and 550 fs.

3.5 Vibronic Coupling Tailoring via Solvation

The results discussed in 3.4 have clearly established the relation between the relative energy of the $1B_u^+$ and $1B_u^-$ states and the strength of the coupling between these states, and how it changes with the carotenoid's conjugation length. An additional way of changing the relative energy of these two electronic states is by using their different interaction with the solvent. The one-electron symmetry properties of polyenes, first used by Pariser[4] and further investigated by Pople and others,[5] distinguish electronic states as so-called *plus* and *minus* ones. While *plus* states are ionic states, *minus* states show a very strong covalent character. This property can be exploited to shift differently the states of carotenoids.[20]

Solvents with large polarizability tend to stabilize the ionic S_2 state and decrease its energy.[53] The same does not happen to covalent electronic states, like the $1A_g^-$, $2A_g^-$, $3A_g^-$ and $1B_u^-$ states, which are barely affected in their energetic position by solvent interaction. The energy shift of ionic states in respect to covalent states can be clearly seen in the steady state absorption spectrum ($1A_g^- \rightarrow 1B_u^+$ transition) as well as in the excited state absorption of the S_1 state ($2A_g^- \rightarrow nB_u^+$ transition).[20]

By carefully choosing the polarizability of the solvent, it is therefore possible to tailor the evolution of the vibrational dynamics. This is demonstrated for lutein ($N \sim 10$) in three different solvents with increasing polarizability (Fig. 9). Lutein in hexane shows a frequency down-shift similar to the one observed for similar open-chain carotenoids (spheroidene and neurosporene). Lutein in benzene, a solvent with a much higher polarizability, shows a completely different evolution of the vibrational frequency in pump-DFWM: A frequency up-shift for both stretching modes of lutein in benzene can be observed, similar to the up-shifts observed in section 3.3 for longer carotenoids like lycopene and spirilloxanthin.

These results reveal two important aspects of the energy levels and their coupling in lutein. The first one is that the separation of $1B_u^-$ and $1B_u^+$ states of lutein in hexane is as close as the separation found for the same states in spheroidene in a much more polarizable solvent (THF), if the vibrational frequency shift is taken as a direct measure of the coupling strength. This illustrates again how different the relative energy between the excited electronic states of open- and closed-chain carotenoids can vary with similar conjugated double bonds.

The second aspect again shows the requirements of energy degeneracy between vibrational levels in the $1B_u^-$ and $1B_u^+$ states in order to observe diabatic mixing. The disappearance of the frequency down-shift when benzene is used as solvent indicates that the $1B_u^+$ is so strongly stabilized and shifted by the solvent, that any kind of coupling between these states is suppressed. This energy shift can be approximated by the shift of the steady state absorption spectrum, which shows for lutein that the energy of the S_2 state decreases almost 400 cm^{-1} in comparison to the $1A_g^-$ when the solvent is shifted from hexane to benzene (see Supporting Information). In this situation the $1B_u^-$ is still below the $1B_u^+$, as Fig. 1 shows for carotenoids with $N \sim 10$, but the individual vibrational levels in each electronic state are not energetically resonant as in hexane.
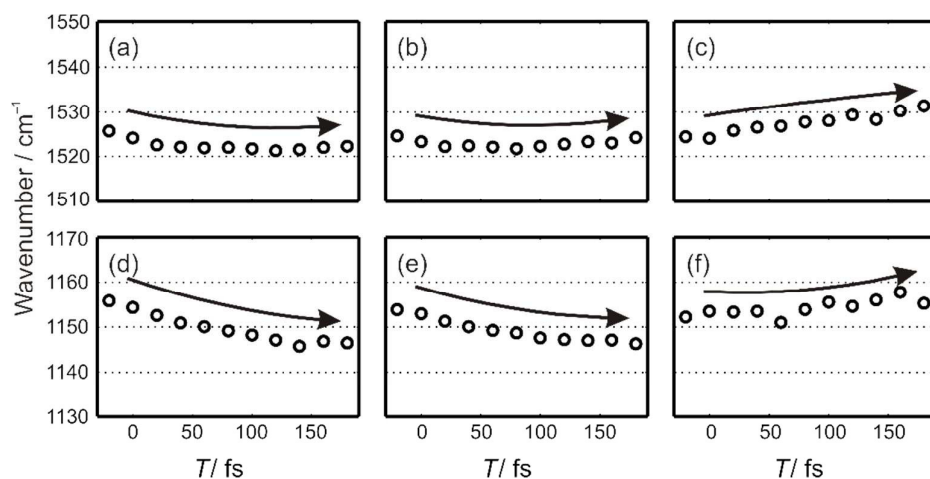
Figure 9- Evolution of the vibrational frequency for the (a)-(c) C=C and (d)-(f) C-C stretching mode for lutein in three different solvents measured with pump-DFWM. From left to the right: hexane, THF and benzene. The arrows are a guide for the eye.

Moreover, the presence of a stronger coupling for non-polarizable solvents also has an effect on the initial population dynamics. A three-component deconvolution with a sequential model of data obtained with transient absorption shows an acceleration of the dynamics with the solvent polarizability. (Fig. 10) While lutein in hexane shows initial time constants of $\tau_1=43\pm5$fs and $\tau_2=35\pm2$fs, the much more polarizable solvent, benzene, leads to faster dynamics with $\tau_1=35\pm5$fs and $\tau_2=23\pm5$fs (see also the Supplementary Information). By comparing these results with the frequency shift show in Fig.9, it can be clearly seen that the presence of diabatic mixing between $1B_u^-$ and $1B_u^+$ states as found for e.g. lutein in hexane leads to slower population dynamics. This is not surprising since a diabatic mixing between states means a loss of pure $B_u^{+/-}$ symmetry property and may lead to complicated electronic potential surfaces and slower internal relaxations. These results raise though very interesting questions for future experiments about the role of diabatic mixing between electronic states of carotenoids embedded on natural light harvesting complexes.
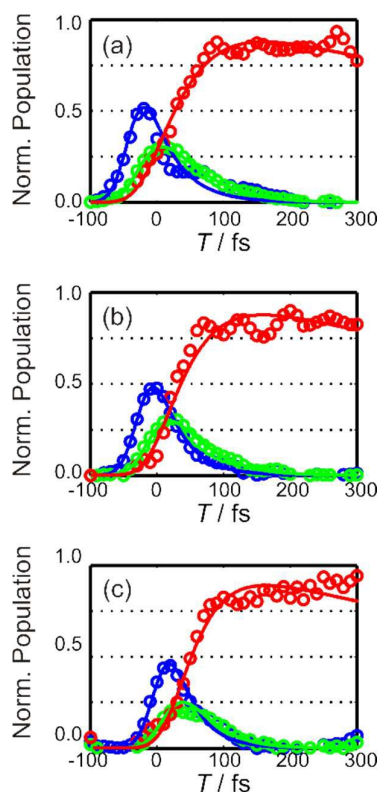
Figure 10- Population evolution for Lutein in (a) hexane, (b) THF and (c) benzene were calculated by global target fitting with a three states sequential model. The original data (circle) was decomposed into S_2 (blue), S_x (green) and S_1 (red) state in the analysis. The fitting models are shown as a solid line.

4. CONCLUSIONS

The experimental findings obtained with multidimensional time-resolved vibrational spectroscopy indicate that the vibrational dynamics directly after the initial excitation of carotenoids is dominated by two different vibronic couplings:

(i)   Diabatic mixing between B_u states takes place only for shorter open-chain carotenoids ($N = 9$ and 10), where the vibrational levels of the $1B_u^+$ and $1B_u^-$ are energetically close (Figure 11). The interaction between these states leads to a typical frequency down-shift after the deactivation of the Franck-Condon region. These results expand and explain the initial experimental observations performed

24

with closed-chain carotenoids with $N = 10$ [19] and shows that diabatic mixing is a general mechanism observed for carotenoids present in light harvesting complexes.

(ii)   Adiabatic coupling between the A_g states is a well-known general feature of the Raman spectra of carotenoids, which is responsible for the generation of the typical S_1 C=C stretching frequency at 1800 cm^{-1}. Our results show, nevertheless, it does not lead to any modification of the vibrational dynamics during $1B_u^+$ deactivation, since adiabatic coupling does not take place between $1B_u^+$ and $2A_g^-$ states. The evolution of the S_1 C=C stretching frequency at 1800 cm^{-1} as well as of other modes for carotenoids without diabatic mixing follows a frequency up-shift due to potential anharmonicity (Figure 11).
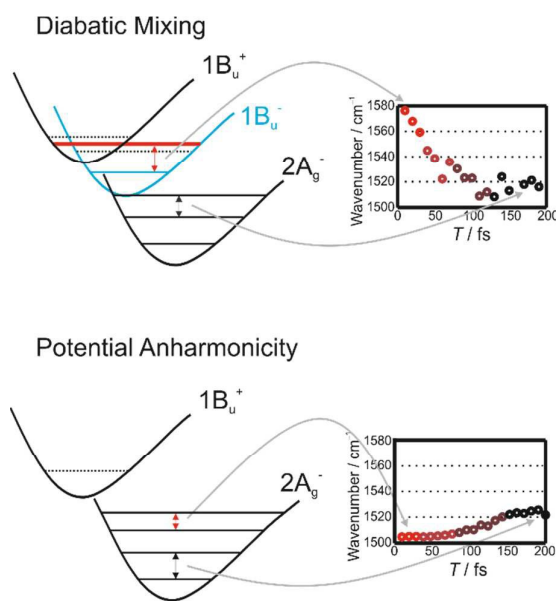
Figure 11- Scheme of vibrational frequencies shifts within the initial 200fs dynamics. Diabatic mixing between $1B_u^+$ and $1B_u^-$ leads to a frequency down-shift during the evolution from the $1B_u^+/1B_u^-$ mixed potential to the $2A_g^-$ potential. The red line in the $1B_u^+/1B_u^-$ mixed potential depicts the shifted vibrational level due to the diabatic mixing. Frequency up-shifts due to the $2A_g^-$ potential anharmonicity can be observed in the initial dynamics when diabatic mixing does not play a role. The intermediate states in the scheme for describing potential anharmonicity were omitted for clarity.

The importance of the energy degeneracy for the strength of the diabatic mixing was further corroborated by fine tuning the energy of the $1B_u^+$ electronic state with respect to the other covalent dark states. By exploiting solvents with different polarizability, the shift of the vibrational frequency, typical for diabatic mixing of nearly degenerate states, was modulated accordingly. The observation of the effect of the coupling between B_u states on the vibrational dynamics here agrees with previous state-of-the-art experimental work in the group of Cerullo on the interplay of population dynamics and solvation effects.[28] In conclusion, the coupling between electronic states is a very important feature in the deactivation of electronic excited states of carotenoids. It not only explains how deactivation depends on the length of the carotenoid chain, but also the role of solvation.

Supporting Information. It contains information on 1. $1800 cm^{-1}$ mode of neurosporene, 2. Absorption spectrum of lutein in different solvents. 3. Accuracy of the Time Constants for the Sequential Model.

REFERENCES

1.   G. A. Worth and L. S. Cederbaum, *Annual Review of Physical Chemistry*, 2004, **55**, 127-158.
2.   G. Orlandi and W. Siebrand, *Chem. Phys. Lett.*, 1972, **15**, 465-468.
3.   G. Orlandi and F. Zerbetto, *Chem. Phys.*, 1986, **108-195**, 187.
4.   R. Pariser, *J. Chem. Phys.*, 1956, **24**, 250-268.
5.   P. Tavan and K. Schulten, *J. Chem. Phys.*, 1986, **85**, 6602-6609.
6.   P. Tavan and K. Schulten, *Phys. Rev. B*, 1987, **36**, 4337-4358.
7.   W. Fuß, Y. Haas and S. Zilberg, *Chem. Phys.*, 2000, **259**, 273-295.
8.   D. W. McCamant, P. Kukura and R. A. Mathies, *J. Phys. Chem. A*, 2003, **107**, 8208-8214.
9.   T. Hornung, H. Skenderovic and M. Motzkus, *Chem Phys Lett*, 2005, **402**, 283-288.
10.   J. Hauer, T. Buckup and M. Motzkus, *J. Phys. Chem. A*, 2007, **111**, 10517-10529.
11.   A. N. Macpherson and T. Gillbro, *J. Phys. Chem. A*, 1998, **102**, 5049-5058.
12.   P. O. Andersson and T. Gillbro, *J. Chem. Phys.*, 1995, **103**, 2509-2519.
13.   A. P. Shreve, J. K. Trautman, T. G. Owens and A. C. Albrecht, *Chem. Phys. Lett.*, 1991, **178**, 89-96.
14.   F. S. Rondonuwu, K. Yokoyama, R. Fujii, Y. Koyama, R. J. Cogdell and Y. Watanabe, *Chem. Phys. Lett.*, 2004, **390**, 314-322.
15.   H. Kandori, H. Sasabe and M. Mimuro, *J. Am. Chem. Soc.*, 1994, **116**, 2671-2672.
16.   D. Kosumi, K. Yanagi, R. Fujii, H. Hashimoto and M. Yoshizawa, *Chem Phys Lett*, 2006, **425**, 66-70.
17.   F. Rondonuwu, Y. Kakitani, H. Tamura and Y. Koyama, *Chem. Phys. Lett.*, 2006, **429**, 234-238.
18.   R. Fujii, T. Ishikawa, Y. Koyama, M. Taguchi, Y. Isobe, H. Nagae and Y. Watanabe, *J Phys Chem A*, 2001, **105**, 5348-5355.
19.   E. Ostroumov, M. G. Müller, C. M. Marian, M. Kleinschmidt and A. R. Holzwarth, *Phys. Rev. Lett.*, 2009, **103**, 108302.
20.   T. Polívka and V. Sundström, *Chem. Rev.*, 2004, **104**, 2021-2071.
21.   T. Polívka and V. Sundström, *Chem. Phys. Lett.*, 2009, **477**, 1-11.
22.   K. Furuichi, T. Sashima and Y. Koyama, *Chem. Phys. Lett.*, 2002, **356**, 547-555.
23.   J.-P. Zhang, T. Inaba, Y. Watanabe and Y. Koyama, *Chem. Phys. Lett.*, 2000, **332**, 351-358.
24.   G. Cerullo, D. Polli, G. Lanzani, S. D. Silvestri, H. Hashimoto and R. J. Cogdell, *Science*, 2002, **298**, 2395-2398.
25.   Y. Koyama, Y. Kakitani, T. Miki, R. Christiana and H. Nagae, *Int. J. Mol. Sci.*, 2010, **11**, 1888-1929.
26.   T. Miki, Y. Kakitani, Y. Koyama and H. Nagae, *Chem. Phys. Lett.*, 2008, **457**, 222-226.
27.   H. Nagae, Y. Kakitani and Y. Koyama, *Chem. Phys. Lett.*, 2009, **474**, 342-351.
28.   M. Maiuri, D. Polli, D. Brida, L. Lüer, A. M. LaFountain, M. Fuciman, R. J. Cogdell, H. A. Frank and G. Cerullo, *Phys. Chem. Chem. Phys.*, 2012, **14**, 6312-6319.
29.   M. Sugisaki, D. Kosumi, K. Saito, R. J. Cogdell and H. Hashimoto, *Phys Rev B*, 2012, **85**, 245408.
30.   H. A. Frank, *The photochemistry of carotenoids*, Kluwer Academic, Dordrecht, Netherlands ; Boston, 1999.
31.   M. Kleinschmidt, C. M. Marian, M. Waletzke and S. Grimme, *Journal of Chemical Physics*, 2009, **130**, 044708.

32.   S. Knecht, C. M. Marian, J. Kongsted and B. Mennucci, *Journal of Physical Chemistry B*, 2013, **117**, 13808-13815.
33.   T. Buckup, J. Hauer, J. Möhring and M. Motzkus, *Arch. Biochem. Biophys.*, 2009, **483**, 219-223.
34.   M. S. Marek, T. Buckup and M. Motzkus, *J. Phys. Chem. B*, 2011, **115**, 8328-8337.
35.   J. P. Kraack, A. Wand, T. Buckup, M. Motzkus and S. Ruhman, *Phys. Chem. Chem. Phys.*, 2013, **15**, 14487.
36.   M. S. Marek, T. Buckup, J. Southall, R. J. Cogdell and M. Motzkus, *The Journal of chemical physics*, 2013, **139**, 074202.
37.   T. Buckup and M. Motzkus, *Annu. Rev. Phys. Chem.*, 2014, **65**, 39-57.
38.   M. Motzkus, S. Pedersen and A. H. Zewail, *J. Phys. Chem.*, 1996, **100**, 5620-5633.
39.   S. Yamaguchi and H.-o. Hamaguchi, *J. Chem. Phys.*, 1998, **109**, 1397-1408.
40.   J.-P. Zhang, T. Inaba, Y. Watanabe and Y. Koyama, *Chem. Phys. Lett.*, 2000, **331**, 154-162.
41.   Q. Zhang, S. A. Kandel, T. A. W. Wasserman and P. H. Vaccaro, *Journal of Chemical Physics*, 1992, **96**, 1640-1643.
42.   J. P. Kraack, T. Buckup and M. Motzkus, *J Phys Chem Lett*, 2013, **4**, 383-387.
43.   J. P. Kraack, T. Buckup and M. Motzkus, *Phys Chem Chem Phys*, 2012, **14**, 13979-13988.
44.   F. Ehlers, M. Scholz, J. Schimpfhauser, J. Bienert, K. Oum and T. Lenzer, *Phys Chem Chem Phys*, 2015, **17**, 10478-10488.
45.   T. Lenzer, F. Ehlers, M. Scholz, R. Oswald and K. Oum, *Phys Chem Chem Phys*, 2010, **12**, 8832-8839.
46.   H. Hashimoto and Y. Koyama, *Chem Phys Lett*, 1989, **154**, 321-325.
47.   H. Nagae, M. Kuki, J. P. Zhang, T. Sashima, Y. Mukai and Y. Koyama, *J Phys Chem A*, 2000, **104**, 4155-4166.
48.   J. P. Kraack, M. Motzkus and T. Buckup, *Journal of Chemical Physics*, 2011, **135**, 224505.
49.   R. Shimada and H.-o. Hamaguchi, *The Journal of chemical physics*, 2014, **140**, 204506.
50.   F. S. Rondonuwu, Y. Watanabe, J.-P. Zhang, K. Furuichi and Y. Koyama, *Chem. Phys. Lett.*, 2002, **357**, 376-384.
51.   H. Hayashi, T. Noguchi, M. Tasumi and G. H. Atkinson, *Biophys. J.*, 1991, **60**, 252-260.
52.   D. W. McCamant, J. E. Kim and R. A. Mathies, *J Phys Chem A*, 2002, **106**, 6030-6038.
53.   P. O. Andersson, T. Gillbro, L. Ferguson and R. J. Cogdell, *Photochemistry and Photobiology*, 1991, **54**, 353-360.

Tabel of Contents Image